Orientation Growth and Magnetic Properties of Electrochemical Deposited Nickel Nanowire Arrays

Yu, Yanlong; Li, Jinpeng; Wang, Jun; Wu, Xige; Yu, Cuiyan; Xu, Tao; Chang, Bingdong; Sun, Hongyu; Arandiyan, Hamidreza

Published in:
Catalysts

Link to article, DOI:
10.3390/catal9020152

Publication date:
2019

Document Version
Publisher's PDF, also known as Version of record

catalysts

MDPI

Communication

Orientation Growth and Magnetic Properties of Electrochemical Deposited Nickel Nanowire Arrays

Yanlong Yu [1,†], Jinpeng Li [2,†], Jun Wang [3], Xige Wu [4], Cuiyan Yu [1], Tao Xu [1], Bingdong Chang [5], Hongyu Sun [5,*] and Hamidreza Arandiyan [6,*]

1 Department of petroleum and chemical engineering, Northeastern Petroleum University, Qinhuangdao 066004, China; ylyu66@126.com (Y.Y.); ycy977900@163.com (C.Y.); tangguoguoaixi@163.com (T.X.)
2 ULVAC Research Center SUZHOU Co., Ltd., Beijing 100176, China; roclie@gmail.com
3 College of chemistry and chemical engineering, Northeastern Petroleum University, Daqing 163318, China; jingxilongyu@163.com
4 Daqing Qing Lu Long Green Technology Company, Daqing 163318, China; dbsydq@126.com
5 National Centre for Nano Fabrication and Characterization, Technical University of Denmark, 2800 Kongens Lyngby, Denmark; bincha@dtu.dk
6 Laboratory of Advanced Catalysis for Sustainability, School of Chemistry, The University of Sydney, Sydney 2006, Australia
* Correspondence: hsun@nanotech.dtu.dk (H.S.); hamid.arandiyan@sydney.edu.au (H.A.)
† The authors contribute equally to this work.

Received: 20 December 2018; Accepted: 31 January 2019; Published: 3 February 2019

Abstract: Highly ordered ferromagnetic metal nanowire arrays with preferred growth direction show potential applications in electronic and spintronic devices. In this work, by employing a porous anodic aluminum oxide template-assisted electrodeposition method, we successfully prepared Ni nanowire arrays. Importantly, the growth direction of Ni nanowire arrays can be controlled by varying the current densities. The crystalline and growth orientation of Ni nanowire arrays show effects on magnetic properties. Single-crystallinity Ni nanowires with [110] orientation show the best magnetic properties, including coercivity and squareness, along the parallel direction of the nanowire axis. The current preparation strategy can be used to obtain other nanowire arrays (such as metal, alloy, and semiconductor) with controlled growth direction in confined space, and is therefore of broad interest for different applications.

Keywords: Nanowire arrays; orientation; electrodeposition; magnetic properties

1. Introduction

With the rapid development of spintronics, information storage and the logical operation based on magnetic domain wall dynamics are proposed [1–5]. By controlling the movement or the injection of domain walls in ferromagnetic nanowire arrays, ultra-high density storage, or ultra-fast logical operation is expected to be achieved. Precise control of the structural parameters, such as size, composition, orientation, and assembly of ferromagnetic nanowires is of importance to obtain the desired functional properties and device performance [6–8]. Lithography is a typical top-down method to fabricate nanowire arrays [9–11]. Nevertheless, expensive equipment and complex fabrication processes hinder the large-scale applications of this technique. In comparison, solution phase synthesis represents one of the most effective and facile routes, in terms of energy consumption and equipment costs, to realize the controllable synthesis of a wide range of nanostructures. Among these methods, template-assisted electrodeposition is a popular way to obtain uniform and highly ordered nanowire arrays [12,13]. The nucleation and growth kinetics of the nanowire arrays in one-dimensional confined

geometry can be tuned by different experimental parameters, including template dimension, electrolyte properties (pH value, composition, additive, and so on), reaction temperature, applied voltage, and the current density [14–17]. In our previous work, we demonstrated that current density can influence the growth direction and crystalline quality of electrodeposited semiconductor nanowire arrays, and further change their photoluminescence properties [18,19].

Porous anodic aluminum oxide (AAO) is a widely used template due to the ideal uniform pore distribution, tunable pore diameters, and facile fabrication process [20]. Combining AAO template with electrodeposition has been studied for decades to synthesize different nanowire arrays; nevertheless, recent years have seen further development in this area, regarding more mechanical understanding in the pore formation [21], fine manipulation of pores, and thus nanostructure configurations [22], syntheses of novel materials [23], and new applications [24]. All of these give new opportunities and development to this *routine* preparation method for nanomaterials.

Although the preparation of Ni nanowire arrays by using template-assisted electrochemical deposition method has been extensively studied [25–31], the control of growth orientation and understanding the mechanism are challenged. In this work, we prepared Ni nanowire arrays by using an AAO template-assisted electrodeposition method. The growth orientation of Ni nanowires is successfully controlled under different current densities. The effect of growth orientation on the magnetic properties of the nanowire arrays embedded in AAO template is studied in detail. This work provides a possible route to understand the electrocrystallization behavior in a confined space, and thus is essential to grow high-quality ferromagnetic nanowire arrays for potential applications in electronic and spintronic devices.

2. Results and Discussion

Figure 1 shows the XRD patterns of the AAO template, as well as Ni nanowires embedded in the AAO template that was prepared at setting current densities. The broad peak of the template demonstrates the amorphous characteristic of Al_2O_3 (Figure 1a). At a lower current density of 1.2 mA/cm^2 (Figure 1b), distinct diffraction peaks were observed, which are identified as (111), (200), (220), and (311) crystalline planes of metal Ni with face-centred cubic phase (JCPDS No. 04-0850). In addition, no other diffraction peaks could be found, suggesting a high phase purity of the Ni nanowires. With the increase of current density to 1.5 mA/cm^2 (Figure 1c) and 2.0 mA/cm^2 (Figure 1d), the relative intensity of the (111), (200), and (311) peaks decreased, while the relative intensity of the (220) peak increased. At the current density of 2.5 mA/cm^2 (Figure 1e), only the (220) peak could be detected, suggesting the Ni nanowires are single crystal with [110] as the growth direction. In addition, the average crystallite size can be estimated from Scherrer formula [32]. At current densities of 1.2 mA/cm^2 (Figure 1b) and 1.5 mA/cm^2 (Figure 1c), the grain sizes calculated by using (111) diffraction peak are ~28.9 nm and 22.9 nm, respectively. With the increasing of current densities, the (220) peak becomes sharper, indicating an increased grain size (>100 nm) that related to (220) plane. Such grain size changing also suggests a preferred orientation transition from [111] to [220].

Additional structure and morphology analysis are studied by electron microscopes. The SEM morphology of a typical AAO template is shown in Figure 2. The pores are ordered and circular, and the average pore diameter is ~30 nm (Figure 2a). In addition, the pores are perpendicular to the surface of template, and the template thickness is around 35 μm (Figure 2b). Figure 2c displays a plan-view SEM image of Ni nanowires prepared at a high current density (2.5 mA/cm^2). Obviously, large-scale ordered nanowires are obtained, and the nanowires grow perpendicular to the substrate. The average size of nanowires is around 2 μm in length and 30 nm in diameter, respectively. In the following studies, we adjusted the deposition time for the employed current densities to have the nanowires possess the same length (~2 μm, the SEM images are not shown here).

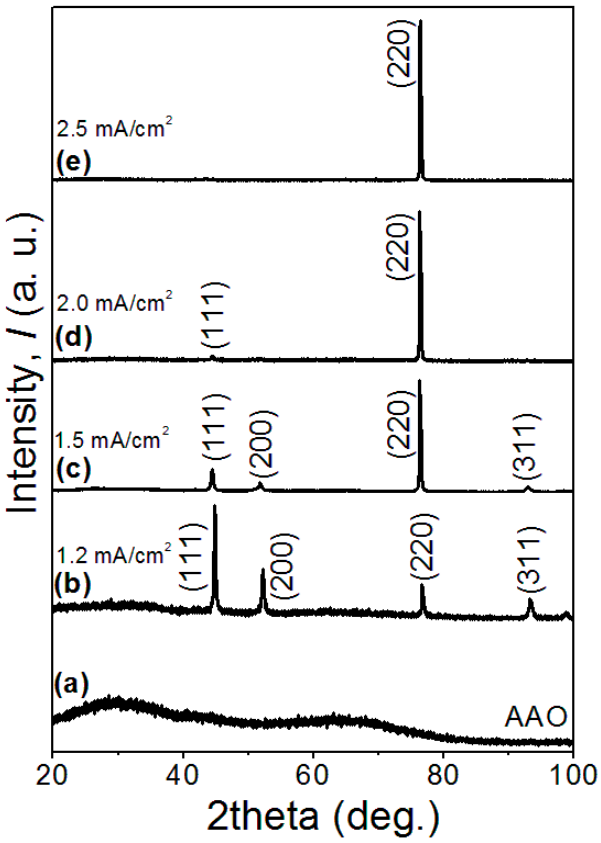

Figure 1. Typical XRD spectra of (a) AAO template, (b–e) Ni nanowire arrays prepared at various current densities (1.2 mA/cm^2~2.5 mA/cm^2). The Ni nanowire arrays that obtained at a low current density (1.2 mA/cm^2) has a polycrystalline structure, while the nanowire arrays grow along the [110] orientation at a higher current density (2.5 mA/cm^2).

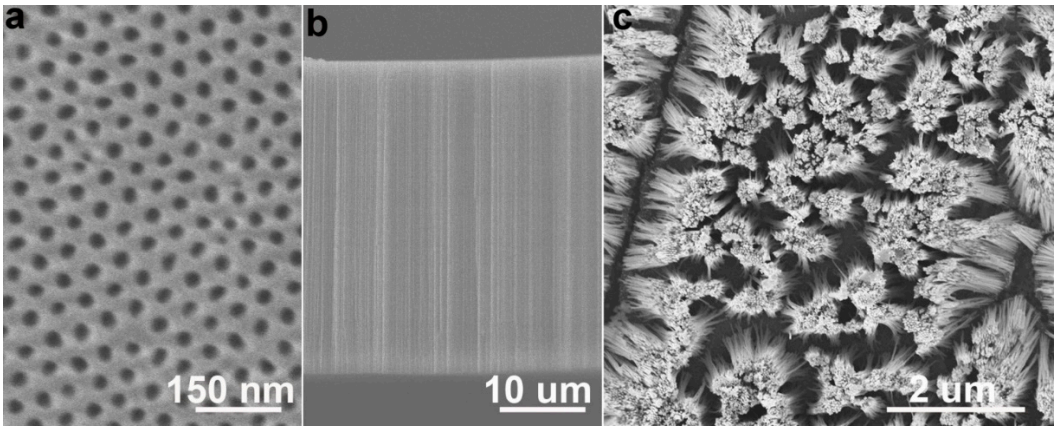

Figure 2. Typical SEM images of a AAO template: (**a**) plan-view, (**b**) view from crossing; (**c**) SEM image of Ni nanowire arrays (current density = 2.5 mA/cm^2).

Typical TEM images of individual Ni nanowires are illustrated in Figure 3. It is obvious that the nanowires show similar diameter of ~30 nm, confirming well-confined growth controlled by the AAO pores. Electron diffraction patterns obtained by the selected area (SAED) clearly indicate a transformation from the polycrystalline structure to single crystalline structure by increasing the current density. In the range of 1.2–2.0 mA/cm^2, the diffraction patterns show polycrystalline ring characteristics. When the current density is 2.5 mA/cm^2, the spotty pattern of single-crystalline structure is observed. The TEM observations coincide with the above XRD analysis.

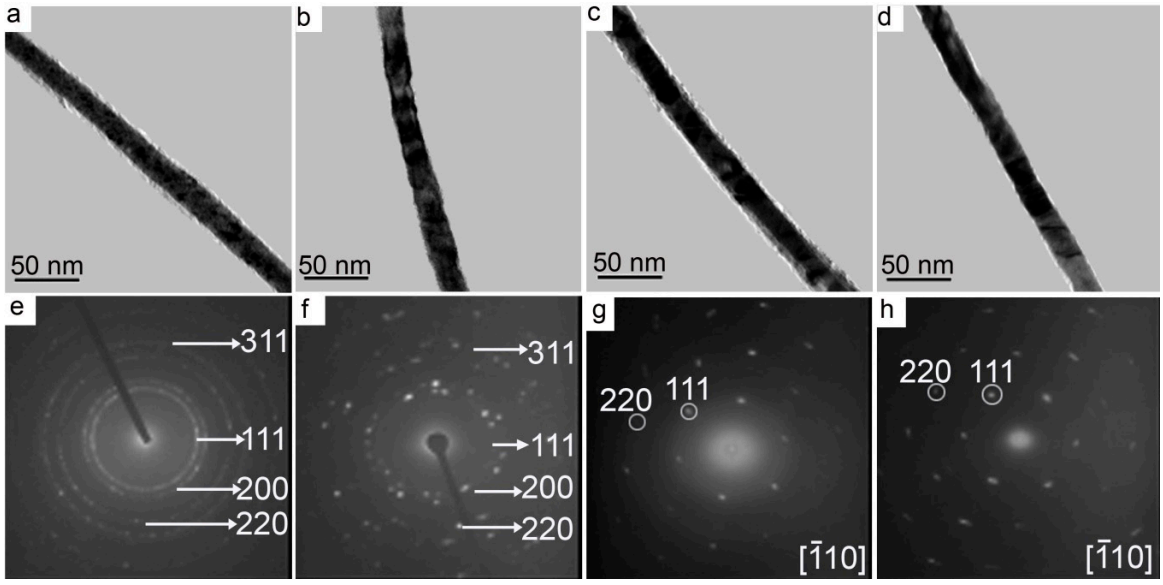

Figure 3. Typical (**a**–**d**) TEM images and (**e**–**h**) corresponding SAED patterns of a single Ni nanowire that deposited under current densities of (**a**,**e**) 1.2 mA/cm^2, (**b**,**f**) 1.5 mA/cm^2, (**c**,**g**) 2.0 mA/cm^2, (**d**,**h**) 2.5 mA/cm^2.

In our previous work, the nanowire growth in a porous template can be described by a modified electrocrystallization model [19,33], of which the critical nucleus size N_c can be expressed as: $N_c = \kappa_n[(1 + \varrho)E_{hkl}/ze\eta]^n$, where $\kappa_n = \lambda_n \exp(-nkr/h)$, λ_n is a constant that is dependent on nucleation dimension (n), z and η are the effective electron number, the overpotential, k and ϱ are parameters, r (radius) and h (height) are the geometry dimensions of 2D critical nucleus, and E_{hkl} is the surface energy of (hkl) crystal face. The E_{hkl} value is related to bonding properties, and it can also be modified by environmental conditions. For example, surface energy can be decreased through selective absorption by different gases or ions [34,35]. For Ni crystals, the maximum difference of the E_{hkl} values for (111), (200), and (220) surfaces is about 0.3–0.4 J/m^2. Therefore, when Ni nanowires are deposited under a low current density, (111), (200), and (220) surfaces form simultaneously due to the similar surface energies, indicating a polycrystalline nature. Under the high current density condition, the high overpotential facilitates the adsorption of hydrogen in the electrolyte ($4H_3O^+ + 4e^- \leftrightarrow 4H_2O + 2H_2$), especially on the facet with high surface energy (such as (220) plane for Ni crystals) [36,37]. This ion adsorption can decrease the surface energy, making it even lower than the pristine low-surface-energy facet (such as (111) plane). In the end, the growth of Ni nanowire arrays is along the [110] direction [18,38]. We did not observe the nanowire arrays with other orientations in the studied current density range; nevertheless, it is anticipated that other orientations could be obtained by changing the surface energy order of different facets, which can be achieved by selecting a suitable current density and surface absorbent. It should be mentioned here that, besides current density, the pH value and temperature can also affect the microstructure of the deposited nanowires [30]. In our experiments, there was no obvious change of the electrolyte temperature. We did not measure the pH value during the deposition process, which, however, is worth investigating in our future work.

We studied the magnetic properties of the Ni nanowires by using a VSM. A magnetic field (H = 5 kOe) is applied along two different directions, i.e., perpendicular ($H_\perp$) or parallel ($H_{//}$) to the nanowire axis direction (Figure 4). The squareness (M_r/M_s) of the recorded hysteresis loops measured with $H_{//}$ is much better than the measurements with $H_\perp$. This clearly demonstrates the strong magnetic anisotropy for the Ni nanowires. No matter the crystallinity of the nanowires, all samples indicate the long axis of the Ni nanowire should be the easy axis for the magnetization, which can be attributed to the 1D characteristic structure of the nanowires (shape anisotropy) [39–41].

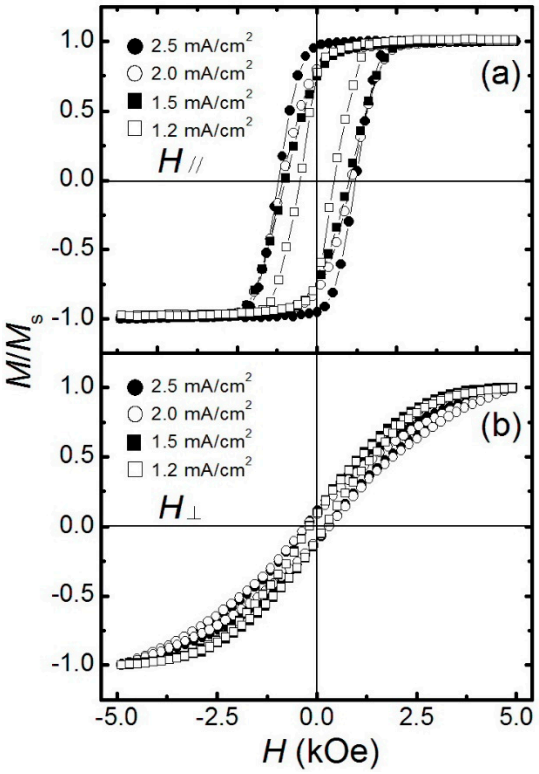

Figure 4. The magnetization hysteresis loops of the samples with the magnetic field applied (**a**) parallel ($H_{//}$) and (**b**) perpendicular ($H_{\perp}$) to the axis direction of the nanowire arrays prepared at various current densities (1.2 mA/cm^2~2.5 mA/cm^2).

The coercivity and M_r/M_s of the nanowire samples deposited at different current densities are summarized as shown in Figure 5. Both coercivity and squareness increased with parallel field by increasing the current density of the electrodeposition. Generally, magnetic anisotropy can be induced by crystal structures, orientation, and shape. Herein, the length of the four Ni nanowire arrays is similar (~2 μm), therefore, the possibility of crystal structures and shape anisotropy induced magnetic property change can be excluded. Additionally, the AAO template confines the nanowire diameter to ~30 nm, all Ni samples can be considered single-domain objects [42]. The sample at 1.2 mA/cm^2 shows a significantly lower coercivity than other samples under the parallel magnetic field. This is caused by its poor crystallinity and small domain size which is confirmed by the XRD and SAED. The broad background and weak peak intensity indicate the nanowire contain amorphous states in its composition which can cause the deterioration of the coercivity. Although the sample at 1.5 mA/cm^2 still shows polycrystalline nature of the materials, the spotty diffraction ring pattern of SAED indicates the crystallinity is improved, and the magnetic domain size is increased to enhance the coercivity [43,44]. When the current density is increased to 2.0 mA/cm^2, the single-crystalline nature of the nanowire further improves the domain size and the coercivity. The sample at the 2.5 mA/cm^2 shows the highest coercivity and the best squareness, indicating the high oriented single-crystalline sample improves ferromagnetic performance of the nanowire along the long axis.

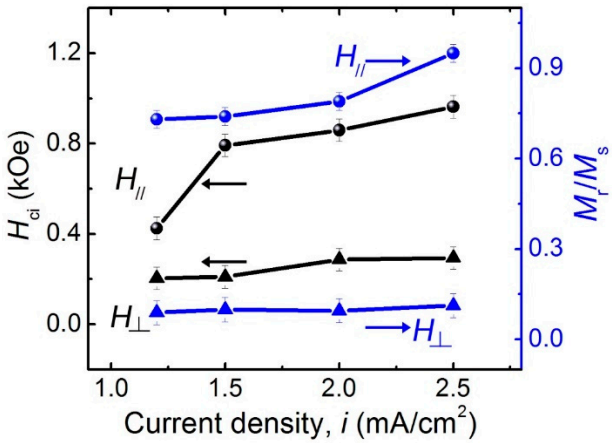

Figure 5. The relationship between coercivity (left, black), squareness (right, blue) of the Ni nanowires and the deposited current densities.

3. Experimental

3.1. Fabrication of AAO Template

The AAO templates were fabricated by a anodization method at 15 °C [45,46]. Firstly, pure aluminum foil (99.99%, with a thickness ~0.5 mm) was cleaned in acetone solution and then annealed in vacuum condition at 500 °C for 2 h. The anodization was firstly operated under a constant voltage of 30 V in oxalic acid solution (0.4 M) for 9 h. The alumina layer produced in the anodization was then removed, and the aluminum plate was anodized for 14 h. After the anodization, we utilized a solution of $SnCl_2$ (0.05 M) to clear away the central aluminum layer. To remove the barrier layer on the bottom side, additional etching was employed by using a phosphoric acid solution (5 wt%) as etchant. Finally, copper film (50 nm in thickness) was sputtered onto one side of the AAO template.

3.2. Electrodeposition of Ni Nanowire Arrays

Ni nanowire arrays were prepared by a constant-current electrodeposition method in a standard two-electrode system. A pure Ni plate (99.9%) and AAO template with copper film were served as the counter and working electrodes, respectively. The electrolyte contained a mixture of nickel sulfate hexahydrate ($NiSO_4 \cdot 6H_2O$, 2.0 M) and boric acid (H_3BO_3, 0.6 M). The current density was set between 1.2 mA/cm^2 and 2.5 mA/cm^2. All the depositions were performed at room temperature.

3.3. Materials Characterization

The crystallographic information and phase structure were analyzed by employing an X-ray diffractometer with Cu-Kα radiation (XRD, D/max-2500/PC, wavelength 1.5418 Å, Rigaku, Tokyo, Japan). The morphology and microstructure were characterizated by a scanning electron microscope (SEM, Merlin, 5 keV, Zeiss, Oberkochen, Germany.) and a transmission electron microscope (TEM, JEM 2010, 200 keV, JEOL, Tokyo, Japan). The magnetic properties were measured with a vibrating sample magnetometer (VSM, Model 7407, magnetic field 5 kOe, LakeShore, Westerville, OH, USA) at room temperature.

4. Conclusions

We have demonstrated the preparation of orientation controlled Ni nanowire arrays by tuning the electrodeposited current density. The single-crystalline nanowire grown at 2.5 mA/cm^2 shows a favourite orientation along [110] direction. The mechanism can be understood by a modified electrocrystallization model. The measurement of magnetic properties indicates the single-crystallinity improved the coercivity and squareness of the Ni nanowires. Our investigation is essential to understand the growth of ferromagnetic nanowires and to explore potential applications in electronic,

spintronic devices, and catalysts. Moreover, the present strategy can also be extended to prepare other nanowire arrays, including metal, alloy, and semiconductors, with controlled growth direction in confined space.

Funding: This research was funded by the National Natural Scientific Foundation of China, grant number 51601037.

Conflicts of Interest: The authors declare no conflict of interest.

References

1. Parkin, S.S.P.; Hayashi, M.; Thomas, L. Magnetic domain-wall racetrack memory. *Science* **2008**, *320*, 190–194. [CrossRef] [PubMed]
2. Allwood, D.A.; Xiong, G.; Faulkner, C.C.; Atkinson, D.; Petit, D.; Cowburn, R.P. Magnetic domain-wall logic. *Science* **2005**, *309*, 1688–1692. [CrossRef] [PubMed]
3. Catalan, G.; Seidel, J.; Ramesh, R.; Scott, J.F. Domain wall nanoelectronics. *Rev. Mod. Phys.* **2012**, *84*, 119–156. [CrossRef]
4. Belashchenko, K.D.; Tchernyshyov, O.; Kovalev, A.A.; Tretiakov, O.A. Magnetoelectric domain wall dynamics and its implications for magnetoelectric memory. *Appl. Phys. Lett.* **2016**, *108*, 132403. [CrossRef]
5. Garg, C.; Yang, S.-H.; Phung, T.; Pushp, A.; Parkin, S.S.P. Dramatic influence of curvature of nanowire on chiral domain wall velocity. *Sci. Adv.* **2017**, *3*, e1602804. [CrossRef]
6. Whitney, T.M.; Searson, P.C.; Jiang, J.S.; Chien, C.L. Fabrication and magnetic properties of arrays of metallic nanowires. *Science* **1993**, *261*, 1316–1319. [CrossRef]
7. Ivanov, Y.P.; Chuvilin, A.; Lopatin, S.; Kosel, J. Modulated magnetic nanowires for controlling domain wall motion: toward 3D magnetic memories. *ACS Nano* **2016**, *10*, 5326–5332. [CrossRef]
8. Grutter, A.J.; Krycka, K.L.; Tartakovskaya, E.V.; Borchers, J.A.; Reddy, K.S.M.; Ortega, E.; Ponce, A.; Stadler, B.J.H. Complex three-dimensional magnetic ordering in segmented nanowire arrays. *ACS Nano* **2017**, *11*, 8311–8319. [CrossRef]
9. Za'bah, N.F.; Kwa, K.S.K.; Bowen, L.; Mendis, B.; O'Neill, A. Top-down fabrication of single crystal silicon nanowire using optical lithography. *J. Appl. Phys.* **2012**, *112*, 024309. [CrossRef]
10. Min, S.-Y.; Kim, T.-S.; Kim, B.J.; Cho, H.; Noh, Y.-Y.; Yang, H.; Cho, J.H.; Lee, T.-W. Large-scale organic nanowire lithography and electronics. *Nat. Commun.* **2013**, *4*, 1773. [CrossRef]
11. Ozel, T.; Bourret, G.R.; Mirkin, C.A. Coaxial lithography. *Nat. Nanotechnol.* **2015**, *10*, 319–324. [CrossRef] [PubMed]
12. Jin, C.G.; Jiang, G.W.; Liu, W.F.; Cai, W.L.; Yao, L.Z.; Yao, Z.; Li, X.G. Fabrication of large-area single crystal bismuth nanowire arrays. *J. Mater. Chem.* **2003**, *13*, 1743. [CrossRef]
13. Wildt, B.; Mali, A.P.; Searson, P.C. Electrochemical template synthesis of multisegment nanowires: fabrication and protein functionalization. *Langmuir* **2006**, *22*, 10528–10534. [CrossRef] [PubMed]
14. Pan, H.; Liu, B.; Yi, J.; Poh, C.; Lim, S.; Ding, J.; Feng, Y.; Huan, C.H.A.; Lin, J. Growth of single-crystalline Ni and Co nanowires via electrochemical deposition and their magnetic properties. *J. Phys. Chem. B* **2005**, *109*, 3094–3098. [CrossRef]
15. Han, X.-F.; Shamaila, S.; Sharif, R.; Chen, J.-Y.; Liu, H.-R.; Liu, D.-P. Structural and magnetic properties of various ferromagnetic nanotubes. *Adv. Mater.* **2009**, *21*, 4619–4624.
16. Yue, G.; Xu, Q.; Meng, G.; He, X.; Han, F.; Zhang, L. Electrochemical synthesis and magnetic properties of single-crystal and netlike poly-crystal Ni nanowire arrays. *J. Alloys Compd.* **2009**, *477*, L30–L34. [CrossRef]
17. Medina, J.D.; Hamoir, G.; Velázquez-Galván, Y.; Pouget, S.; Okuno, H.; Vila, L.; Encinas, A.; Piraux, L. Large magnetic anisotropy enhancement in size controlled Ni nanowires electrodeposited into nanoporous alumina templates. *Nanotechnology* **2016**, *27*, 145702. [CrossRef] [PubMed]
18. Sun, H.Y.; Yu, Y.L.; Li, X.H.; Li, W.; Li, F.; Liu, B.T.; Zhang, X.Y. Controllable growth of electrodeposited single-crystal nanowire arrays: The examples of metal Ni and semiconductor ZnS. *J. Cryst. Growth* **2007**, *307*, 472–476. [CrossRef]
19. Sun, H.Y.; Li, X.H.; Chen, Y.; Li, W.; Li, F.; Liu, B.T.; Zhang, X.Y. The control of the growth orientations of electrodeposited single-crystal nanowire arrays: a case study for hexagonal CdS. *Nanotechnology* **2008**, *19*, 225601. [CrossRef]

20. Masuda, H.; Fukuda, K. Ordered metal nanohole arrays made by a two-step replication of honeycomb structures of anodic alumina. *Science* **1995**, *268*, 1466–1468. [CrossRef]
21. Li, Z.; Li, Y.; Li, S.; Wu, J.; Hu, X.; Ling, Z.; Jin, L. A modified quantitative method for regularity evaluation of porous AAO and related intrinsic mechanisms. *J. Electrochem. Soc.* **2018**, *165*, E214–E220. [CrossRef]
22. Wen, L.; Xu, R.; Mi, Y.; Lei, Y. Multiple nanostructures based on anodized aluminium oxide templates. *Nat. Nanotechnol.* **2017**, *12*, 244–250. [CrossRef] [PubMed]
23. Ashley, M.J.; O'Brien, M.N.; Hedderick, K.R.; Mason, J.A.; Ross, M.B.; Mirkin, C.A. Templated synthesis of uniform perovskite nanowire arrays. *J. Am. Chem. Soc.* **2016**, *138*, 10096–10099. [CrossRef] [PubMed]
24. Xue, J.; Zhou, Z.-K.; Wei, Z.; Su, R.; Lai, J.; Li, J.; Li, C.; Zhang, T.; Wang, X.-H. Scalable, full-colour and controllable chromotropic plasmonic printing. *Nat. Commun.* **2015**, *6*, 8906. [CrossRef] [PubMed]
25. Tan, M.; Chen, X.Q. Growth mechanism of single crystal nanowires of fcc metals (Ag, Cu, Ni) and hcp metal (Co) electrodeposited. *J. Electrochem. Soc.* **2012**, *159*, K15–K20. [CrossRef]
26. Cortés, A.; Riveros, G.; Palma, J.L.; Denardin, J.C.; Marotti, R.E.; Dalchiele, E.A.; Gómez, H. Single-crystal growth of nickel nanowires: influence of deposition conditions on structural and magnetic properties. *J. Nanosci. Nanotechnol.* **2009**, *9*, 1992–2000. [CrossRef] [PubMed]
27. Wang, X.W.; Fei, G.T.; Xu, X.J.; Jin, Z.; Zhang, L.D. Size-dependent orientation growth of large-area ordered Ni nanowire arrays. *J. Phys. Chem. B* **2005**, *109*, 24326–24330. [CrossRef] [PubMed]
28. Wang, X.W.; Fei, G.T.; Chen, L.; Xu, X.J.; Zhang, L.D. Orientation-controllable growth of Ni nanowire arrays with different diameters. *Electrochem. Solid-State Lett.* **2007**, *10*, E1–E3. [CrossRef]
29. Dellis, S.; Christoulaki, A.; Spiliopoulos, N.; Anastassopoulos, D.L.; Vradis, A.A. Electrochemical synthesis of large diameter monocrystalline nickel nanowires in porous alumina membranes. *J. Appl. Phys.* **2013**, *114*, 164308. [CrossRef]
30. Barriga-Castro, E.D.; García, J.; Mendoza-Reséndez, R.; Prida, V.M.; Luna, C. Pseudo-monocrystalline properties of cylindrical nanowires confinedly grown by electrodeposition in nanoporous alumina templates. *RSC Adv.* **2017**, *7*, 13817–13826. [CrossRef]
31. Prida, V.M.; Hernández-Vélez, M.; Cervera, M.; Pirota, K.; Sanz, R.; Navas, D.; Asenjo, A.; Aranda, P.; Ruiz-Hitzky, E.; Batallán, F.; et al. Magnetic behaviour of arrays of Ni nanowires by electrodeposition into self-aligned titania nanotubes. *J. Magn. Magn. Mater.* **2005**, *294*, e69–e72. [CrossRef]
32. Ashby, M.F.; Ferreira, P.J.; Schodek, D.L. *Nanomaterials, Nanotechnologies and Design: An Introduction for Engineers and Architects*; Butterworth-Heine-Mann: Oxford, UK, 2009; p. 288.
33. Paunovic, M.; Schlesinger, M. *Fundamentals of Electrochemical Deposition*, 2nd ed.; Wiley-Interscience: New York, NY, USA, 2006; p. 114.
34. Wang, Z.L.; Gao, R.P.; Nikoobakht, B.; El-Sayed, M.A. Surface reconstruction of the unstable {110} surface in gold nanorods. *J. Phys. Chem. B* **2000**, *104*, 5417–5420. [CrossRef]
35. Peng, X.; Manna, L.; Yang, W.; Wickham, J.; Scher, E.; Kadavanich, A.; Alivisatos, A.P. Shape control of CdSe nanocrystals. *Nature* **2000**, *404*, 59–61. [CrossRef] [PubMed]
36. Liu, Y.; Huang, Y.C.; Xiao, Z.B.; Reng, X.W. Study of adsorption of hydrogen on Al, Cu, Mg, Ti surfaces in Al alloy melt via first principles calculation. *Metals* **2017**, *7*, 21. [CrossRef]
37. Löber, R.; Hennig, D. Interaction of hydrogen with transition metal fcc (111) surfaces. *Phys. Rev. B* **1997**, *55*, 4761. [CrossRef]
38. Pan, H.; Sun, H.; Poh, C.; Feng, Y.; Lin, J. Single-crystal growth of metallic nanowires with preferred orientation. *Nanotechnology* **2005**, *16*, 1559–1564. [CrossRef]
39. Sun, L.; Hao, Y.; Chien, C.-L.; Searson, P.C. Tuning the properties of magnetic nanowires. *IBM J. Res. Dev.* **2005**, *49*, 79–102. [CrossRef]
40. Yu, C.Y.; Yu, Y.L.; Sun, H.Y.; Xu, T.; Li, X.H.; Li, W.; Gao, Z.S.; Zhang, X.Y. Enhancement of the coercivity of electrodeposited nickel nanowire arrays. *Mater. Lett.* **2007**, *61*, 1859–1862. [CrossRef]
41. Song, Y.; Lu, W.; Xu, Y.; Shi, J.; Fang, X. Growth of single-crystalline Co_7Fe_3 nanowires via electrochemical deposition and their magnetic properties. *J. Alloys Compd.* **2015**, *652*, 179–184. [CrossRef]
42. Kartopu, G.; Yalçın, O.; Choy, K.-L.; Topkaya, R.; Kazan, S.; Aktaş, B. Size effects and origin of easy-axis in nickel nanowire arrays. *J. Appl. Phys.* **2011**, *109*, 033909. [CrossRef]
43. Chen, C.H.; Knutson, S.J.; Shen, Y.; Wheeler, R.A.; Horwath, J.C.; Barnes, P.N. The effect of particle size on coercivity and crystallinity of $SmCo_5$. *Appl. Phys. Lett.* **2011**, *99*, 012504. [CrossRef]

44. Shaterabadi, Z.; Soltanian, S.; Koohbor, M.; Salimi, A.; Servati, P. Modification of microstructure and magnetic properties of electrodeposited Co nanowire arrays: A study of the effect of external magnetic field, electrolyte acidity and annealing process. *Mater. Chem. Phys.* **2015**, *160*, 389–397. [CrossRef]
45. Chen, Y.; Yan, H.; Li, X.H.; Li, W.; Zhang, J.W.; Zhang, X.Y. Assembly of Ni/γ-Fe_2O_3 shell/core nanowires. *Mater. Lett.* **2006**, *60*, 245–247. [CrossRef]
46. Sun, H.Y.; Li, X.H.; Li, W.; Li, F.; Liu, B.T.; Zhang, X.Y. Low-temperature synthesis of wurtzite ZnS single-crystal nanowire arrays. *Nanotechnology* **2007**, *18*, 115604. [CrossRef]